A study of the carbon distribution in bainitic ferrite

Irina Pushkareva, Juan Macchi, Babak Shalchi-Amirkhiz, Fateh Fazeli, Guillaume Geandier, Frederic Danoix, Julien Teixeira, Sebastien Y.P. Allain, Colin Scott

A study of the carbon distribution in bainitic ferrite

Irina Pushkareva [a,*], Juan Macchi [b], Babak Shalchi-Amirkhiz [a], Fateh Fazeli [a], Guillaume Geandier [b], Frederic Danoix [c], Julien Da Costa Teixeira [b], Sébastien Yves Pierre Allain [b], Colin Scott [a]

[a] CanmetMaterials, Natural Resources Canada, 183 Longwood Road South, Hamilton, ON L8P 0A5, Canada
[b] Institut Jean Lamour, UMR CNRS-UL 7198, 54011 Nancy, France
[c] Normandie Université, UNIROUEN, INSA Rouen, CNRS, Groupe de Physique des Matériaux, 76000 Rouen, France

ARTICLE INFO

Keywords:
bainitic steels
Carbon
Atom probe tomography, electron energy loss spectroscopy (EELS)
X-ray diffraction (XRD)

ABSTRACT

The carbon distribution in bainitic ferrite (BF) of two carbide-free bainite alloys isothermally transformed at three different temperatures was studied using a unique combination of in-situ high energy X-ray diffraction (HEXRD), atom probe tomography (APT) and electron energy loss spectroscopy (EELS). Results from all three techniques are consistent and unambiguously confirm the presence of significant excess carbon levels in BF, even in these low nominal carbon (0.22 wt.%) steels. The carbon concentration in BF decreases as the transformation temperature increases, but remains significant up to 430 °C. Further, statistical analysis indicates that the excess carbon content does not follow a normal distribution. APT reconstructions suggest that much (but not all) of the excess carbon is segregated to defects or clusters. No clear evidence for bainite tetragonality was observed. Surprisingly, the addition of a strong carbide forming element (vanadium) in solid solution did not influence the carbon distribution in BF.

The presence of carbon in bainitic ferrite at concentrations higher than those predicted by para-equilibrium theories has been intensively investigated over the past few decades. The most convincing experimental evidence for this excess carbon comes from atom probe tomography (APT) [1–5] and high energy *in-situ* synchrotron X-ray diffraction (HEXRD) experiments [4,6–8] of high silicon carbide-free bainite (CFB) steels. A comprehensive review of the available data can be found in [9].

Quantifying carbon distributions at very dilute concentrations offers a challenge for both of these techniques. APT permits individual atom counting with excellent spatial resolution (<1 nm^3) and detection limits (about 10 ppm at.). However, the sampled volume is relatively small. Even in the newest instruments it is typically limited to 100 nm x 100 nm x (100 to 500) nm, significantly less than one single austenite grain. In contrast, transmission mode HEXRD probes volumes of the order of 1 mm^3 i.e. at least 10^4 austenitic grains. APT data inevitably suffers from sampling variability and doubts about the representativity of the studied volume but does provide a reliable direct measurement of the local carbon content. HEXRD on the other hand has the disadvantage that carbon concentrations must be inferred indirectly from lattice parameter measurements. These are subject to influences from other sources such as the presence of residual stresses, the effect of alloying elements or, more importantly in the case of bainitic ferrite, possible tetragonality of the lattice. A critical summary of the potential limitations of both techniques can be found in [10].

While the presence of excess carbon in CFB has been established, the conditions under which this occurs (composition, transformation temperature) have not yet been clearly identified. Further, the degree to which the ferrite lattice is actually supersaturated is not settled, as carbon in bainitic ferrite can be segregated to clusters, phase boundaries, nano-precipitates or dislocation cores. In the majority of reported studies high nominal carbon contents (0.6 wt.% < C_0 < 1 wt.%) were employed to lower the martensite transformation start temperature (M_s) and promote bainitic transformations at very low temperatures where the kinetics are slower and the concentration of excess carbon is higher [1–4,6,8], thus reducing the experimental difficulties. Fewer investigations have been done on industrially important low carbon steels [3,5,7]. Finally, the effect of the presence in solid solution of carbide forming elements such as V has not been systematically studied.

In this paper we report on a study where, for the first time, a third independent analysis technique, Electron Energy Loss Spectroscopy (EELS) in the TEM has been employed in parallel with APT and in situ HEXRD to study the carbon distribution in two low carbon carbide-free

bainite (CFB) alloys during and after isothermal transformation. This combination of complementary techniques covers a sub-nano- to micro- to millimeter scale range and is unique in that it provides carbon measurements from all matrix phases present; bainitic ferrite, retained austenite and martensite.

The two CFB alloys investigated here were cast as 50 kg ingots in a VIM furnace and hot rolled on the pilot scale rolling mill at CanmetMATERIALS. Table 1 shows the measured chemical compositions of the reference (Ref) and added vanadium (Ref+*V*) steels. Isothermal transformations at 375 °C, 400 °C and 430 °C were carried out following the thermal paths shown in Fig. 1a in a Bahr DIL 805 deformation dilatometer. The isothermal hold time was 600 s. A description of the resulting microstructures and mechanical properties has been reported elsewhere [11].

In-situ transmission HEXRD experiments were carried out on the Petra P07 beam line at DESY (Deutsche Synchrotron) in Hamburg, which is equipped with a similar Bahr dilatometer. The 100 keV monochromatic X-ray source was focused to a beam with a 400 μm x 400 μm cross-section and diffractograms were recorded on a 2-D Perkin-Elmer charge coupled device (CCD) placed 1 m after the sample so that at least 5 diffraction rings from each phase could be imaged. The data acquisition frequency was ~ 10 Hz. The Debye-Scherrer rings were integrated using the Fit2D software [12] and then analysed with a full Rietveld refinement method. Pseudo-Voigt functions were fitted to the diffraction peaks using the FullProf code [13] to determine the lattice parameters and phase fractions. The austenite carbon content C_γ was obtained from the relative lattice dilatation Δa_γ between each measured lattice parameter value, a_m and a reference lattice parameter, a_{tr} determined at the transformation temperature just before the start of the bainitic transformation. The austenite carbon enrichment ΔC_γ can be obtained [14]:

$$\Delta a_\gamma = a_m - a_{tr} = k_C \Delta C_\gamma \quad (1)$$

where the constant k_C is 0.00105 nm/(at.%)C [15]. C_γ is then the sum of ΔC_γ and the nominal carbon content C_0. Planar TEM thin foils were prepared directly from the synchrotron specimens and were analysed in a Technai Osiris 200 keV X-FEG (S)TEM equipped with a Gatan Enfina (FS1) EELS analysis system. The carbon content in martensite, bainite and retained austenite phases was measured by EELS using a modified standards based second difference acquisition technique developed by the authors [16]. The established detection limit for carbon using this method is better than 0.04 wt.%. and recent improvements indicate an estimated detection limit of 0.02–0.03 wt.%. APT investigations were carried out on a CAMECA LEAP 4000 HR system operated in voltage mode at 50 K, with a pulse fraction of 20% and a repetition rate of 200 kHz. A total of 42 successful runs were completed on tips prepared by electropolishing using the standard two stage method. C atoms were identified on mass spectra at m/n = 6 amu for C++, 12 amu for C+, 18 amu for (C3)++, 24 amu for an equal amount of (C2)+ and (C4)++ (thus counted as 3 individual C atoms on average per count) and at 36 amu for (C3)+. Data were processed using IVAS® 3.8.10 software, and reconstructions obtained with k = 4.1 and ξ=1.65.

Fig. 1a shows the evolution of the bcc fraction for the two alloys during three thermal cycles with isothermal transformations at 375 °C, 400 °C and 430 °C. All transformations were 95% complete within 160 s. The final austenite phase fraction was not modified by the addition of V, being 12% at 375 °C, 14% at 400 °C and 19% at 430 °C for both steels. Less than 1% martensite formed during final cooling after transformation at 375 °C and 400 °C. At 430 °C, 2.5% martensite formed in the Ref alloy and 5.9% in Ref+*V*. As is clear in Fig. 1b, less carbon is partitioned to retained austenite at higher transformation temperatures. This results in reduced austenite stability and hence increased martensite formation during final cooling, as observed in Fig. 1a. The partitioning of carbon to retained austenite lags behind the transformation and this effect is strongest at lower temperatures where C_γ is still increasing more than 400 s after bainite completion. Overall, the presence of V appears to reduce the amount of carbon that partitions to austenite, but the temperature dependence of this effect is not clear.

Table 1
Chemical compositions of the studied steels in wt.%.

Steel	C	Mn	Si	Mo	V	AI	N
Ref	0.22	2.2	1.8	0.2	–	0.01	0.0028
Ref+*V*	0.22	2.2	1.8	0.2	0.15	0.01	0.0027

TEM investigations revealed a matrix phase consisting of lath bainite with thin (~100 nm) films of retained austenite. These films occasionally showed a partial transformation to martensite, particularly in samples with higher transformation temperatures. Fig. 2 contains a bright field TEM image from the Ref alloy transformed at 430 °C showing an area containing all three phases. A detailed investigation of the precipitation state in bainite and in austenite was previously carried out [11]. Although a few coarse undissolved V(C,N) particles were detected, no evidence of nano-precipitates nucleated during the bainitic transformation was seen, in accordance with the predictions of kinetic precipitation modeling. Thus, the majority of V remained in solid solution throughout the transformation. No cementite reflections were present in any of the HEXRD patterns. However, in the TEM a few isolated cementite particles in the sub 10 nm diameter size range were detected in bainitic ferrite.

Atom probe data for both alloys was obtained for transformations at 375 °C and 430 °C. The reconstructions shown in Fig. 2 illustrate typical carbon distributions from all three phases. Retained austenite showed a uniform carbon distribution, fresh martensite contained a high density of nano-clusters (the martensite start temperature M_s is 375°*C* for these alloys so some degree of auto-tempering is expected) and bainitic ferrite consisted of some uniform regions interspersed with zones of strongly segregated carbon, possibly associated with planar defects (lath boundaries) and/or dislocations.

The results for the average carbon measurements in austenite (C_γ), martensite (C_α'), and bainitic ferrite (C_b) using all three techniques are summarised in Table 2 and graphically for the bainite and austenite phases in Fig. 3. C_b from HEXRD was determined from the carbon balance between fcc and bcc phases such that:

$$C_0 = C_b(1 - F_\gamma) + C_\gamma F_\gamma \quad (2)$$

This is valid up until the end of isothermal holding, assuming no other phases are present at this point. C_b represents the total amount of carbon present in bainitic ferrite and is independent of its chemical state (segregated, precipitated or in solution). This value can be directly compared with EELS data, as EELS measures the total number of carbon atoms in the analysed volume in all chemical states. Finally, for consistency, C_b from APT includes the carbon in the segregated regions in bainitic ferrite i.e. no attempt was made to differentiate carbon in true solid solution from segregated carbon as proposed by [3].

Where appropriate we have included error bars in Fig. 3 that represent the standard deviation of the results obtained (i.e. not the measurement error) from EELS and APT. This is possible as the number of measurements carried out was sufficiently high. The uncertainty in the HEXRD data is mainly due to the error in determining the phase fractions and is very small (<1%).

The three independent analysis techniques give broadly consistent results. The only obvious outliers are the APT results for austenite that are based on one or at most two islands detected and therefore probably not statistically representative. APT quantitative measurements of carbon have shown anomalous directional enrichment in ferrite due to trajectory aberrations [17] and non-directional enrichment in martensite when multiple detection events result in the preferential loss of Fe_{56}^{2+} ions [18]. In fact the latter error is systematic in APT datasets. For the experimental conditions employed in this study, it has been

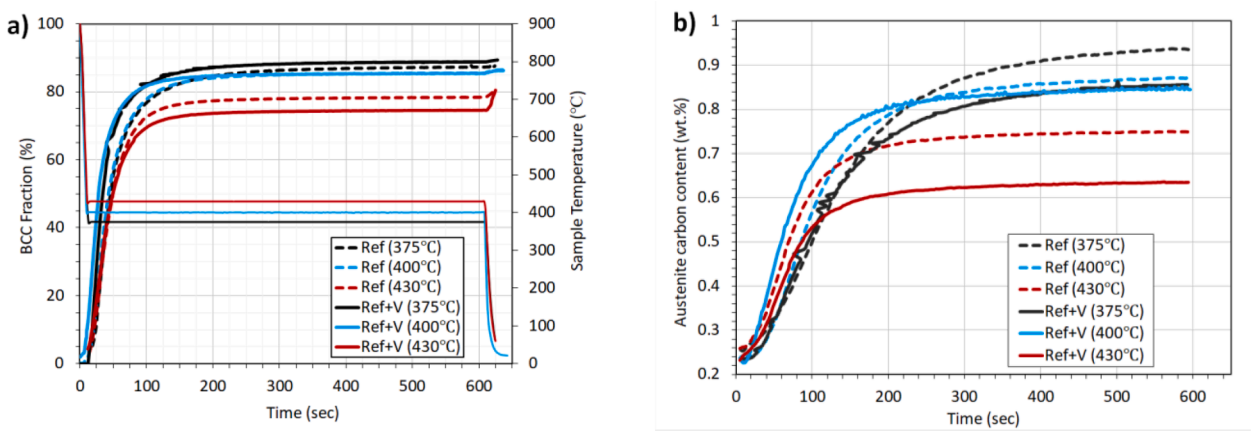

Fig. 1. a) HEXRD data showing isothermal bainitic transformation kinetics at 375 °C, 400 °C and 430 °C of Ref and Ref+*V* alloys. b) The corresponding evolutions of the mean austenite carbon contents.

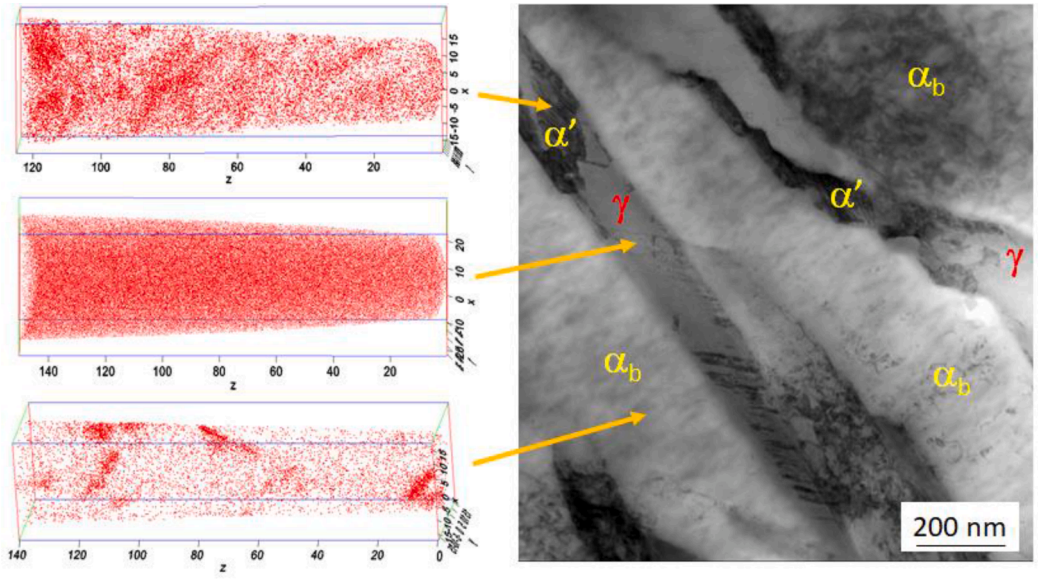

Fig. 2. TEM bright field image (right) of the Ref alloy transformed at 430 °C. The APT reconstructions (left) show typical carbon distributions for martensite (α'), austenite (γ) and bainitic ferrite (α_b).

Table 2
A comparison of HEXRD, EELS and APT data for average carbon measurements in austenite, martensite and bainitic ferrite. The figures in brackets indicate the number of regions/APT tips analysed.

Alloy	Transformation Temperature	C_γ HEXRD (wt.%)	C_γ EELS (wt.%)	C_γ APT (wt.%)	$C_{\alpha'}$ EELS (wt.%)	C_b HEXRD (wt.%)	C_b EELS (wt.%)	C_b APT (wt.%)
Ref	375 °C	0.94	0.98 (9)	1.82 (2)	0.70 (1)	0.12	0.09 (12)	0.11 (12)
Ref	400 °C	0.87	1.20 (7)	–	0.78 (4)	0.11	0.13 (4)	–
Ref	430 °C	0.75	0.69 (8)	1.17 (1)	0.49 (5)	0.08	0.07 (10)	0.05 (7)
Ref+V	375 °C	0.86	0.90 (9)	1.45 (2)	0.36 (3)	0.14	0.10 (13)	0.08 (12)
Ref+V	400 °C	0.85	0.83 (10)	–	0.63 (9)	0.11	0.10 (3)	–
Ref+V	430 °C	0.63	0.73 (8)	0.80 (1)	0.46 (7)	0.09	0.06 (5)	0.04 (9)

measured to be less than 5% relative in bcc (martensite and bainitic ferrite) and less than 2% relative in fcc (austenite). Including the effect of this overestimation does not change the APT values given in Table 2, and is significantly smaller in amplitude than the scatter of measured carbon content in each individual atom probe specimen, as reported in Fig. 3. The average carbon content in both bainitic ferrite and in retained austenite decreases as the transformation temperature increases, except for the EELS measurements of the Ref alloy at 400 °C which show a lot of scatter. The bainitic ferrite carbon concentration remains well above the para-equilibrium prediction at all temperatures, and no obvious influence of vanadium additions at any of the studied temperatures can be discerned. This is rather surprising as vanadium in solid solution is known to decrease the bainitic transformation start temperature in low carbon bainite [19]. As expected, the mean carbon content in martensite $C_{\alpha'}$ is lower than in residual austenite, but very few regions of martensite were detected so the temperature dependence of $C_{\alpha'}$ could not be determined.

The dispersion in the bainitic ferrite carbon content data from both

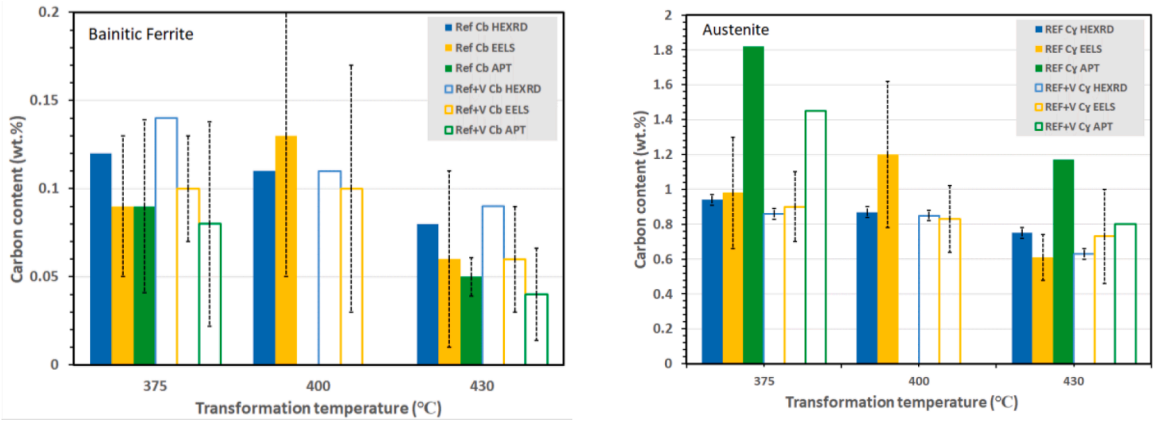

Fig. 3. Graphical representation of the data in Table 2 for bainitic ferrite (left) and retained austenite (right).

EELS and from APT is examined in more detail in Fig. 4a. Here, the individual carbon measurements from the Ref alloy transformed at 375 °C were sorted into bins of 0.01 wt.% in width and then plotted as cumulative distributions. The data was then fitted with error functions to compare the median (C_{50}) and maximum and minimum (C_{10} and C_{90}) values. C_{50} for both EELS and APT is 0.073 wt.%, which is significantly lower than the average values (0.09 wt.% for EELS and 0.11 wt.% for APT). This implies that the excess carbon in bainitic ferrite does not follow a normal distribution and would be better described by a log normal curve. It is known that nano-bainite lath widths follow a log-normal distribution [6] so it is possible that the excess carbon content correlates with lath width. C_{10} lies between 0.02 and 0.03 wt.% and C_{90} is 0.13–0.14 wt.%, reflecting the wide range of the local carbon segregations in bainitic ferrite.

The results from this study (solid points) are compared with the existing literature data (open points) for low carbon bainitic steels with similar compositions [5,7,20] in Fig. 4b. Note that the data from the Ref alloy have been omitted for clarity. The T_0' line calculated for the Ref alloy is also shown (Ref + V is very similar). The agreement between different authors and techniques is generally good. Regarding the carbon excess in bainitic ferrite, it appears that HEXRD systematically predicts higher contents than both APT and EELS. The error in the austenite lattice parameter determination is very low, and the conversion to carbon content via Eq. (1) has been validated many times. However, Eq. (1) does not take into account the effect of hydrostatic transformation stresses on retained austenite films. When martensite is formed, these tend to be compressive [16] and thus could lead to an underestimation of C_γ by up to 20% in the worst case scenario [21]. Consequently, from Eq. (2) the HEXRD measurements for C_b in Fig. 4b would be overestimated. In practice, the long isothermal hold time will allow for significant stress relaxation of the softer austenite phase [22] and it is not expected that the effect of internal stresses on the lattice parameter is more than 10% of the measured variation by the end of transformation. This is borne out by the good agreement between $C\gamma$ (HEXRD) and $C\gamma$ (EELS) as the latter is not sensitive to elastic stresses. In theory, if the final stress state in austenite is anisotropic, then the magnitude of the effect could be studied by comparing lattice parameter measurements from different diffraction peaks. Unfortunately, deconvoluting the effects of stress from the larger variations introduced by the wide distribution of carbon contents in individual austenite islands [11] is likely to be impractical. This leads on to questions on the accuracy of the phase fraction determination. For bcc ferrite that error is very low (<1%), but many workers have shown that bainite in high carbon steels may have significant lattice tetragonality [2,6]. Indeed, the extended solubility of the bct lattice is one way to explain the presence of excess carbon. If this were the case then the bainitic phase fraction calculated assuming a bcc structure could be in error. There are two important objections to tetragonality in low carbon bainite: a) there is no detectable asymmetry or splitting in any of the X-ray diffraction peaks; b) it has been shown that as-quenched martensite with much higher carbon contents up to 0.5 wt.% is not tetragonal [23] (although the latter point is still being debated [24]). Nevertheless, the influence of bainitic ferrite tetragonality was investigated. Indeed, a slightly better adjustment of the Rietveld fitting parameters was obtained when a bct structure was used. However, this actually introduced a small increase in the HEXRD C_b values that further widened the discrepancy with the EELS and APT

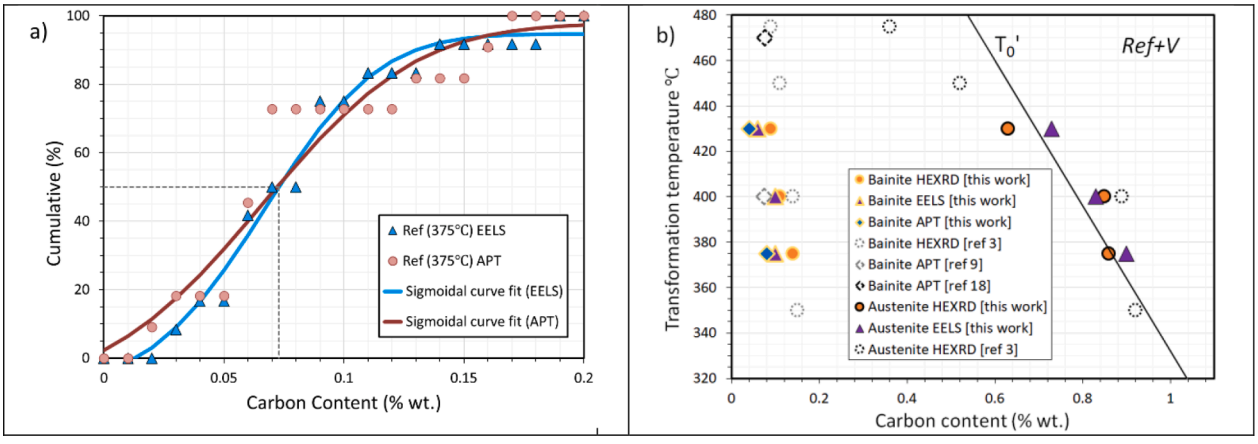

Fig. 4. a) Statistical analysis of the distribution of EELS and APT carbon contents for Ref transformed at 375 °C. b) A comparison of the present results for Ref+*V* (solid points) with the literature data (open points) for fully bainitic low C alloys.

data.

In conclusion, we have used three independent techniques operating at very different scale lengths to investigate the carbon distribution in the constituent phases of two CFB steels. Very consistent results were obtained from all three methods, proving that a large fraction of carbon remains trapped in bainitic ferrite even at higher transformation temperatures (430 °C) and low nominal carbon contents (0.2 wt.%). Statistical analysis of EELS and APT data shows a wide range of local carbon contents in different bainite laths and indicates that the excess carbon content does not follow a normal distribution and would be better described by a log normal curve. These findings could have an impact on the accuracy of previous studies based on observations from lower numbers of APT tips. Surprisingly, the presence of vanadium in solid solution was shown to have a negligible effect on the distribution of carbon in bainitic ferrite, and a very weak effect in retained austenite. The influence of possible tetragonality of the bainite lattice on the reliability of the HEXRD data was considered, however fitting the diffractograms with a bct structure did not provide any definite justification for tetragonality in these low carbon alloys. This, taken together with the lack of any detectable X-ray peak asymmetry/splitting, suggests that any lattice tetragonality in low carbon bainitic ferrite is not significant.

Declaration of Competing Interest

The authors declare that they have no known competing financial interests or personal relationships that could have appeared to influence the work reported in this paper.

Acknowledgements

The authors would like to express their gratitude to the Canadian Office of Energy Research and Development (OERD) and to the LABEX DAMAS (ANR-11-LABX-008–01) Lorraine, France for their support for this work. The synchrotron experiments were carried out at DESY PETRA III in Hamburg, Germany and the authors would like to thank the P07 beamline scientists and engineers. Lorraine Unversité d'Excellence is gratefully acknowledged for Juan Macchi's PhD support. The APT work was carried out under the GENESIS experimental platform. GENESIS is supported by the Région Haute-Normandie, the Métropole Rouen Normandie, the CNRS via LABEX EMC, and the French National Research Agency as a part of the program "Investissements d'avenir" with the reference ANR-11-EQPX-0020. Professors Hatem Zurob and Yves Bréchet are warmly thanked for many interesting and stimulating discussions on the bainitic transformation. Finally, the contribution of the technical staff at CanmetMATERIALS is greatly appreciated.

References

[1] F.G. Caballero, M.K. Miller, A.J. Clarke, C. Garcia-Mateo, Scr. Mater. 63 (2010) 442–445.
[2] C. Garcia-Mateo, J.A. Jimenez, H.-.W. Yen, M.K. Miller, L. Morales-Rivas, M. Kuntz, S.P. Ringer, J.-.R. Yang, F.G. Caballero, Acta Mater 91 (2015) 162–173.
[3] R. Rementeria, J.D. Poplawsky, M.M. Aranda, W. Guo, J.A. Jimenez, C. Garcia-Mateo, F.G. Caballero, Acta Mater 125 (2017) 359–368.
[4] R. Rementeria, J.A. Jimenez, S.Y.P. Allain, G. Geandier, J.D. Poplawsky, W. Guo, E. Urones-Garrote, C. Garcia-Mateo, F.G. Caballero, Acta Mater 133 (2017) 333–345.
[5] Z. Xiong, D.R.G. Mitchell, A.A. Saleh, E.V. Pereloma, Metall. Mater. Trans. A Phys. Metall. Mater. Sci. 49 (2018) 5925–5929.
[6] S. Gaudez, J. Teixeira, S. Denis, G. Geandier, S.Y.P. Allain, Mater. Charact. (2022) 185.
[7] C. Rampelberg, S.Y.P. Allain, G. Geandier, J. Teixeira, F. Lebel, T. Sourmail, JOM 73 (2021) 3181–3194.
[8] H.J. Stone, M.J. Peet, H.K.D.H. Bhadeshia, P.J. Withers, S.S. Babu, E.D. Specht, Proc. R. Soc. A Math. Phys. Eng. Sci. 464 (2008) 1009–1027.
[9] E.V. Pereloma, Mater. Sci. Technol. (United Kingdom) 32 (2016) 99–103.
[10] H.K.D.H. Bhadeshia, Mater. Sci. Technol. (United Kingdom) 31 (2015) 758–763.
[11] I. Pushkareva, B. Shalchi-Amirkhiz, S.Y.P. Allain, G. Geandier, F. Fazeli, M. Sztanko, C. Scott, Metals (Basel) 10 (2020).
[12] http://www.esrf.eu/computing/scientific/FIT2D/.
[13] J. Rodríguez-Carvajal, Phys. B Phys. Condens. Matter 192 (1993) 55–69.
[14] S.Y.P. Allain, G. Geandier, J.-.C. Hell, M. Soler, F. Danoix, M. Gouné, Metals (Basel) 7 (2017).
[15] L. Cheng, A. Böttger, T.H. de Keijser, E.J. Mittemeijer, Scr. Metall. Mater. 24 (1990) 509–514.
[16] C.P. Scott, J. Drillet, Scr. Mater. 56 (2007) 489–492.
[17] Y. Kobayashi, J. Takahashi, K. Kawakami, Ultramicroscopy 111 (2011) 600–603.
[18] G. Miyamoto, K. Shinbo, T. Furuhara, Scr. Mater. 67 (2012) 999–1002.
[19] F. Fazeli, B.S. Amirkhiz, C. Scott, M. Arafin, L. Collins, Mater. Sci. Eng. A 720 (2018) 248–256.
[20] I. Timokhina, H. Beladi, X.-.Y. Xiong, P.D. Hodgson, Metall. Mater. Trans. A Phys. Metall. Mater. Sci. 44 (2013) 5177–5191.
[21] S.Y.P. Allain, S. Gaudez, G. Geandier, J.-.C. Hell, M. Gouné, F. Danoix, M. Soler, S. Aoued, A. Poulon-Quintin, Mater. Sci. Eng. A 710 (2018) 245–250.
[22] D. Lohe, O. Vohringer, Handb. Residual Stress Deform. Steel, ASM INTERNATIONAL (2002) 54–69.
[23] B. Hutchinson, J. Hagström, O. Karlsson, D. Lindell, M. Tornberg, F. Lindberg, M. Thuvander, Acta Mater 59 (2011) 5845–5858.
[24] Y. Lu, H. Yu, R.D. Sisson, Mater. Sci. Eng. A 700 (2017) 592–597.